times solar[5], but to move $\sim 10^7 M_\odot$ of gas inward and to a position >3 kpc above the disk requires more energy than seems available.

A number of authors (see ref. 9 for an overview), have proposed that the Local Group (a cluster of galaxies, of which our Galaxy is a member) is filled with hydrogen clouds with typical hydrogen masses of $10^7 M_\odot$. Adding large amounts of dark matter (10 times as much mass as in hydrogen) could make such clouds stable[22]. In the early universe, these mini-galaxies would pick up heavy elements from the then-nearby large galaxies as the latter vigorously formed stars. Complex C could be such an object, whose orbit brought it close to the Milky Way at the present time. A problem with this model is that similar clouds were not detected in other galaxy groups during a sensitive survey done at Arecibo[23].

A more probable origin was proposed by Oort[24], who argued that the Milky Way is still forming. In this model, much gas was left over after the Milky Way's original formation, and this gas slowly accretes over time. Complex C (and a few other HVCs) would be among the few still-to-be-accreted objects. Its heavy-element content is then understood as a contamination created after it started interacting with gas in the Galactic halo.

Alternatively, HVCs like complex C may consist of gas tidally stripped from nearby dwarf galaxies when the latter's orbit brought them near the Milky Way. The heavy elements would then have been formed in the dwarf. These dwarfs could subsequently have evolved into the present dwarf spheroidal galaxies[25], or their stars might have merged with those of the Milky Way. That such processes still operate is shown by the presence of the Magellanic stream[26], a tidal tail torn out of the Small Magellanic Cloud 2 Gyr ago. Combining the theoretical understanding of the chemical evolution and formation of the Milky Way with the constraints set by observations of other galaxy groups, the current content of the Local Group as well as the position, velocity and metallicity of complex C, we conclude that rather than having been assembled in the early universe, it is more probable that the formation of the Milky Way is still continuing. This is fed by gas either left over from the original formation of the Milky Way or stripped from Local Group dwarf galaxies. □

1. Van den Bergh, S. The frequency of stars with different metal abundances. *Astron. J.* **67,** 486–490 (1962).
2. Giovagnoli, A. & Tosi, M. Chemical evolution models with a new stellar nucleosynthesis. *Mon. Not. R. Astron. Soc.* **273,** 499–504 (1995).
3. Pagel, B. E. J. *Nucleosynthesis and Chemical Evolution of Galaxies* (Cambridge Univ. Press, 1997).
4. Skillman, E. D., Bomans, D. J. & Kobulnicky, H. A. Interstellar medium abundances in the Pegasus dwarf irregular galaxy. *Astrophys. J.* **474,** 205–216 (1997).
5. Rudolph, A. L., Simpson, J. P., Haas, M. R., Erickson, E. F. & Fich, M. Far-infrared abundance measurements in the outer galaxy. *Astrophys. J.* **489,** 94–101 (1997).
6. Ferguson, A. M. N., Gallagher, J. S. & Wyse, R. F. G. The extreme outer regions of disk galaxies. I. Chemical abundances of HII regions. *Astron. J.* **116,** 673–690 (1998).
7. Lu, L., Sargent, W. L. W. & Barlow, T. A. The N/Si abundance ratio in 15 damped Lyα galaxies: implications for the origin of nitrogen. *Astron. J.* **115,** 55–61 (1998).
8. Pettini, M., Ellison, S. L., Steidel, C. C. & Bowen, D. V. Metal abundances at z < 1.5: fresh clues to the chemical enrichment history of damped Lyα systems. *Astrophys. J.* **510,** 576–589 (1999).
9. Wakker, B. P. & van Woerden, H. High-velocity clouds. *Annu. Rev. Astron. Astrophys.* **35,** 217–266 (1997).
10. Savage, B. D. & Sembach, K. R. Interstellar abundances from absorption-line observations with the Hubble Space Telescope. *Annu. Rev. Astron. Astrophys.* **34,** 279–329 (1996).
11. Lu, L. *et al.* The metallicity and dust content of HVC 287.5 + 22.5 + 240: evidence for a Magellanic Clouds origin. *Astron. J.* **115,** 162–167 (1998).
12. Reynolds, R. J., Tufte, S. L., Haffner, L. M., Jaehnig, K. & Percival, J. W. The Wisconsin H-alpha Mapper (WHAM): A brief review of performance characteristics and early scientific results. *Publ. Astron. Soc. Aust.* **15,** 14–18 (1998).
13. Hartmann, D. & Burton, W. B. *Atlas of Galactic Neutral Hydrogen* (Cambridge Univ. Press, 1997).
14. Wakker, B. P. *et al.* in *Stromlo Workshop on High-velocity Clouds* (eds Gibson, B. K. & Putman, M. E.) 26–37 (ASP Conf. Ser. 166, Astronomical Soc. of the Pacific, San Francisco, 1999).
15. Anders, E. & Grevesse, N. Abundances of the elements—Meteoritic and solar. *Geochim. Cosmochim. Acta* **53,** 197–214 (1989).
16. van Woerden, H., Peletier, R. F., Schwarz, U. J., Wakker, B. P. & Kalberla, P. M. W. in *Stromlo Workshop on High-velocity Clouds* (eds Gibson, B. R. & Putman, M. E.) 1–25 (ASP Conf. Ser. 166, Astronomical Soc. of the Pacific, San Francisco, 1999).
17. van Woerden, H., Schwarz, U. J., Peletier, R. F., Wakker, B. P. & Kalberla, P. M. W. A confirmed location in the Galactic halo for the high-velocity cloud 'Chain A'. *Nature* **400,** 138–141 (1999).
18. Snowden, S. L., Egger, R., Finkbeiner, D. P., Freyberg, M. J. & Plucinsky, P. P. Progress on establishing the spatial distribution of material responsible for the 1/4 kev soft x-ray diffuse background local and halo components. *Astrophys. J.* **493,** 715–729 (1998).
19. Wolfire, M. G., McKee, C. F., Hollenbach, D. & Tielens, A. G. G. M. The multiphase structure of the galactic halo: high-velocity clouds in a hot corona. *Astrophys. J.* **453,** 673–684 (1995).
20. Wakker, B. P., Murphy, E. M., van Woerden, H. & Dame, T. M. A sensitive search for molecular gas in high-velocity clouds. *Astrophys. J.* **488,** 216–223 (1997).
21. Bregman, J. N. The galactic fountain of high-velocity clouds. *Astrophys. J.* **236,** 577–591 (1980).
22. Blitz, L., Spergel, D., Teuben, P., Hartmann, D. & Burton, W. B. High velocity clouds: building blocks of the Local Group. *Astrophys. J.* **514,** 818–843 (1999).
23. Zwaan, M. A., Briggs, F. H., Sprayberry, D. & Sorar, E. The HI mass function of galaxies from a deep survey in the 21-cm line. *Astrophys. J.* **490,** 173–186 (1997).
24. Oort, J. H. The formation of galaxies and the origin of the high velocity hydrogen. *Astron. Astrophys.* **7,** 381–404 (1970).
25. Yanny, B. & York, D. G. Emission-line objects near quasi-stellar object absorbers. III Clustering and colors of moderate redshift HII regions. *Astrophys. J.* **391,** 569–576 (1992).
26. Gardiner, L. T. & Noguchi, M. N-body simulations of the Small Magellanic Cloud and the Magellanic Stream. *Mon. Not. R. Astron. Soc.* **278,** 191–208 (1996).
27. Haffner, L. M., Reynolds, R. J. & Tufte, S. L. WHAM observations of Hα, SII, and NII toward the Perseus Arm: probing the physical conditions of the WIM. *Astrophys. J.* **523,** 223–233 (1999).
28. Verner, D. A., Barthel, P. D. & Tytler, D. Atomic data for absorption lines from the ground level at wavelengths greater than 228 Å. *Astron. Astrophys.* **108,** 287–340 (1994).
29. Wakker, B. P., van Woerden, H., Schwarz, U. J., Peletier, R. F. & Douglas, N. G. The Ca+ abundance of HVC complex C. *Astron. Astrophys.* **306,** L25–L28 (1996).

....

Demonstrating the viability of universal quantum computation using teleportation and single-qubit operations

Daniel Gottesman*† & Isaac L. Chuang‡

* Theoretical Astrophysics T-6, MS B-288, Los Alamos National Laboratory, Los Alamos, New Mexico 87545, USA

† Microsoft Research, One Microsoft Way, Redmond, Washington 87545, USA

‡ IBM Almaden Research Center, 650 Harry Road, San Jose, California 95120, USA

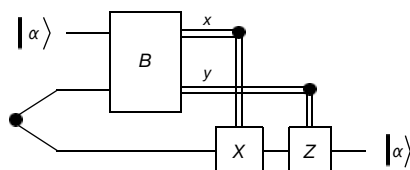...

Algorithms such as quantum factoring[1] and quantum search[2] illustrate the great theoretical promise of quantum computers; but the practical implementation of such devices will require careful consideration of the minimum resource requirements, together with the development of procedures to overcome inevitable residual imperfections in physical systems[3–5]. Many designs have been proposed, but none allow a large quantum computer to be built in the near future[6]. Moreover, the known protocols for constructing reliable quantum computers from unreliable components can be complicated, often requiring many operations to produce a desired transformation[3–5,7,8]. Here we show how a single technique—a generalization of quantum teleportation[9]—reduces resource requirements for quantum computers and unifies known protocols for fault-tolerant quantum computation. We show that single quantum bit (qubit) operations, Bell-basis measurements and certain entangled quantum states such as Greenberger–Horne–Zeilinger (GHZ) states[10]—all of which are within the reach of current technology—are sufficient to construct a universal quantum computer. We also present systematic constructions

for an infinite class of reliable quantum gates that make the design of fault-tolerant quantum computers much more straightforward and methodical.

Quantum teleportation is a scheme by which the state of a qubit can be transported from one point to another by communicating just two classical bits, provided that the sender and the receiver have previously shared halves of a specific two-qubit entangled state. In detail, this is how it works (Fig. 1): a single-qubit state $|\alpha\rangle = a|0\rangle + b|1\rangle$ is prepared, along with a two-qubit entangled state known as an 'Einstein–Podolsky–Rosen' (EPR) state, $|\Psi\rangle = (|00\rangle + |11\rangle)/\sqrt{2}$. The top two qubits, $|\alpha\rangle$ and one qubit of $|\Psi\rangle$, belong to the sender, who measures them in the Bell basis (see Fig. 1 legend). No matter what the input state $|\alpha\rangle$ is, xy is a uniformly distributed random two-bit classical result[11]. This measurement leaves the third qubit, belonging to the receiver, in the state $R_{xy}|\alpha\rangle$, where R_{xy} is either the identity (no transformation) if $xy = 00$, or a single qubit Pauli operation $R_{10} = X$ (a bit flip $|a\rangle \rightarrow |a \oplus 1\rangle$), $R_{01} = Z$ (a phase flip $|a\rangle \rightarrow (-1)^a|a\rangle$), or $R_{11} = Y$ (bit + phase flip $|a\rangle \rightarrow i(-1)^a|a \oplus 1\rangle$)[12]. To complete the teleportation the sender transmits the two classical bits xy to the receiver, who uses them to apply a correction procedure $R_{xy}^{\dagger}$, which is just the inverse of R_{xy}, thus reconstructing an output $|\alpha\rangle$ identical to the original input.

We now consider several features of this procedure which help the intuitive understanding of the result we report here. Teleportation utilizes a specific entangled state $|00\rangle + |11\rangle$ as a resource in accomplishing its aims; what happens when this state is faulty? In general, the teleportation procedure would fail, but sometimes it would fail in a useful manner. If $|\Psi\rangle$ is replaced by $U|\Psi\rangle$, where U is some non-trivial quantum operation, the teleportation procedure produces an output which is not identical to the input. We show below that for certain U, the procedure can be modified so that it produces precisely $U|\alpha\rangle$, that is, the output is a transformed version of the input, where the transformation is determined by the pre-computed entangled state used by the procedure. We shall describe this act as teleporting a state 'through' U. The important points are that (1) the transformation U is potentially useful—it could be an otherwise difficult-to-implement logic gate, (2) the modified tele-portation procedure is simple—it does not require complicated gates, and (3) the resource $U|\Psi\rangle$ can be reliably constructed, even using unreliable gates.

An example illustrates how this works. The Hadamard gate $H = \frac{1}{\sqrt{2}}\begin{bmatrix} 1 & 1 \\ 1 & -1 \end{bmatrix}$ is an important elementary operation for quantum computers, but it cannot be constructed from the Pauli gates X, Y and Z. It turns out that H can be accomplished using teleportation. Instead of $|\Psi\rangle$, use $(I \otimes H)|\Psi\rangle$ as the input entangled state; $I \otimes H$ means 'do nothing to the first qubit, and apply H to the second qubit'. This second qubit is the one possessed by the receiver. The
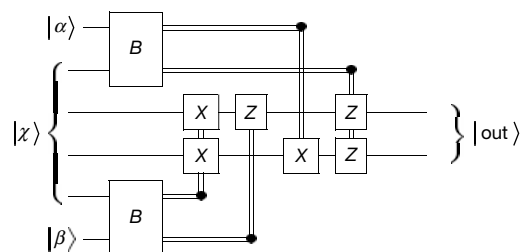
first step of the usual teleportation procedure leaves the receiver with the qubit $HR_{xy}|\alpha\rangle$. We note that H appears to have been performed after R_{xy} even though in practice the Bell-basis measurement is done long after the preparation of $(I \otimes H)|\Psi\rangle$; this time-reversal is a property of using entangled states[5,13]. This seems to be rather inconvenient, because what we really want is $H|\alpha\rangle$. But it happens that $HR_{xy} = R_{x'y'}H$; the Hadamard gate, when commuted through a Pauli gate, produces a Pauli gate. It may be a different gate, but no matter—we know a priori what the classical mapping between xy and $x'y'$ is (in fact, in this case, $x'y' = xy$), and thus when the receiver applies $R_{x'y'}^{\dagger}$ the output state $H|\alpha\rangle$ is obtained, as desired.

A more useful and important gate is the controlled-NOT (CNOT) gate, which acts on two qubits, a control and a target qubit, and flips the target whenever the control qubit is a $|1\rangle$ ($|a, b\rangle \rightarrow |a, a \oplus b\rangle$). We can teleport a state through a CNOT using the quantum circuit shown in Fig. 2. This can be verified by direct computation, but it is easier to understand by realizing that $|\chi\rangle$ can be created by simply performing a CNOT on two EPR pairs (Fig. 3). Combining this circuit with the circuit in Fig. 2, we can see what is happening. Two input qubits are teleported through the CNOT; the correction now depends on four classical bits instead of two. This construction enables CNOT gates to be performed between two qubits, using only classically controlled single-qubit operations, prior entanglement, and Bell-basis measurements. As any quantum computation can be performed using single-qubit operations and CNOT gates[14], this demonstrates an alternative universal set of operations for quantum computation, which does not require any two-qubit operation except the measurement. Moreover, the entangled state $|\chi\rangle$ that is used as a resource can be readily created from two pairs of GHZ[10] states (Fig. 3).

Generalizing this procedure allows us to construct an entire hierarchy of gates through which states can be teleported, and in a fault-tolerant fashion. It is no accident that H and CNOT transform Pauli gates into Pauli gates; the set of gates which does so is known as the Clifford group. It is important in the theory of quantum error-correcting codes and fault-tolerance[5,15]. We now define precisely what operations U can be constructed via teleportation, and how this is done reliably.

Consider an n-qubit state $|\psi\rangle$, in which each qubit is encoded using a stabilizer code, such as the 7-qubit CSS code[16,17]. 0 and 1 shall now represent the corresponding encoded qubit states. Let $|\Psi^n\rangle$ be the $2n$-(encoded) qubit Bell state $(|00\rangle + |11\rangle)^{\otimes n}$ (normalizations suppressed for clarity), rearranged so that the first n labels (the

Figure 1 Quantum circuit for teleportation. Time proceeds from left to right, and < denotes the EPR state $|\Psi\rangle$. The double wires carry classical bits, and the single wires, qubits. The box B represents measurement in the Bell basis; that is, if the two qubits entering B are found to be $|00\rangle + |11\rangle$ (leaving out the $\sqrt{2}$ normalization for clarity), then the outputs $xy = 00$; for $|01\rangle + |10\rangle$, $xy = 10$; for $|00\rangle - |11\rangle$, $xy = 01$; and for $|01\rangle - |10\rangle$, $xy = 11$; one of the four possibilities is guaranteed to be true because the states form a complete basis for all possible two-qubit states. Measurement, in its guise as an interface between the quantum and classical worlds, is generally considered to be an irreversible operation, destroying quantum information and replacing it with classical information. But this circuit demonstrates that in certain carefully designed cases this need not be true, as teleportation uses measurement to transfer states from one place to another.

Figure 2 Quantum circuit for teleporting two qubits through a controlled-NOT gate. The output is $|\text{out}\rangle = \text{CNOT}|\beta\rangle|\alpha\rangle$, where the inputs $|\alpha\rangle = a|0\rangle + b|1\rangle$ and $|\beta\rangle = c|0\rangle + d|1\rangle$ are two arbitrary single qubit states. The CNOT gate has $|\beta\rangle$ as its control, and $|\alpha\rangle$ as its target. The special entangled state $|\chi\rangle$ is $[(|00\rangle + |11\rangle)|00\rangle + (|01\rangle + |10\rangle)|11\rangle]/2$. We recall that multiple qubits can be teleported simply by replicating instances of the single-qubit procedure. Normally, for two qubits, the receiver would obtain the state $R_{x_1y_1}R_{x_2y_2}|\beta, \alpha\rangle$, but because we have replaced the usual EPR pairs by $|\chi\rangle$, the receiver instead obtains $\text{CNOT}R_{x_1y_1}R_{x_2y_2}|\beta, \alpha\rangle$. Now, just as with the Hadamard gate, CNOT has the fortunate property that $\text{CNOT}R_{x_1y_1}R_{x_2y_2} = R_{x'_1y'_1}R_{x'_2y'_2}\text{CNOT}$. This means that the receiver can again apply a modified correction procedure (shown here) to obtain $\text{CNOT}|\beta, \alpha\rangle$.
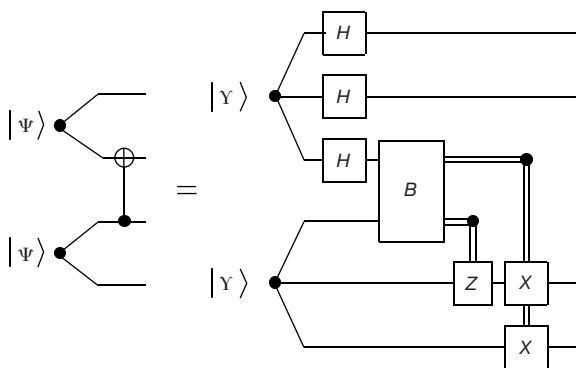
Figure 3 Quantum circuit to create the $|\chi\rangle$ state. It uses two EPR pairs (left) or two GHZ states $|\Upsilon\rangle = (|000\rangle + |111\rangle)/\sqrt{2}$ (right). H is the Hadamard gate.

Figure 4 Quantum circuit to perform U in a fault-tolerant manner using quantum teleportation. In general, this works for any $U \in C_k$, defined as $C_k = \{U|UC_1U^\dagger \subseteq C_{k-1}\}$. Then $R'_{xy} \in C_{k-1}$. $|\Psi_U^n\rangle$ must also be prepared fault-tolerantly. To do this, we note that the state $|\Psi^n\rangle$ is the +1 eigenvector of the $2n$ operators $X_i \otimes X_i$ and $Z_i \otimes Z_i$ (where X_i and Z_i are X and Z, respectively, acting on the ith upper or lower qubit). A computation shows that $|\Psi_U^n\rangle$ is therefore the +1 eigenvector of the operators $M_i = X_i \otimes UX_iU^\dagger$ and $N_i = Z_i \otimes UZ_iU^\dagger$. Furthermore, the eigenvalues of these $2n$ operators completely determine the state, so if all these operators have eigenvalue +1, the state actually is the desired one. Therefore, to produce $|\Psi_U^n\rangle$, measure the operators M_i and N_i, which are in the Clifford group C_2. If the eigenvalue of operator M_i is −1, perform the Pauli operation $Z_i \otimes I$; if the operator N_i has eigenvalue −1, perform $X_i \otimes I$. These operators anticommute with M_i and N_i, so move the state from the −1 eigenspace into the +1 eigenspace, resulting in the state $|\Psi_U^n\rangle$. The hard part of the preparation is measuring M_i and N_i fault-tolerantly, but this can be done by adapting a trick of Shor's[7]. Although the precise set of gates which form C_k is still under investigation, it is known that every C_k contains interesting gates not in an earlier C_k, such as the $\pi/2^k$ rotations, which appear in Shor's factoring algorithm[1]. The union of the C_ks is therefore infinite, even for a fixed number of qubits.

upper qubits) represent qubits from half of each EPR pair, and the last n (the lower qubits) the other halves. In other words, $(I \otimes U)|\Psi^n\rangle$ (where I is the identity on n qubits) is U acting on the lower qubits of all the EPR pairs.

The goal of fault-tolerant computation is to perform logical operations using quantum gates while restricting the propagation of errors among the physical qubits, which can compromise the code's ability to correct errors. The usual method for doing this is to only perform transversal gates on the code—that is, gates which interact qubits in one code block only with corresponding qubits in other code blocks. While errors may then propagate between blocks, they cannot propagate within blocks, so a single faulty gate can only cause a single error in any given block of the code.
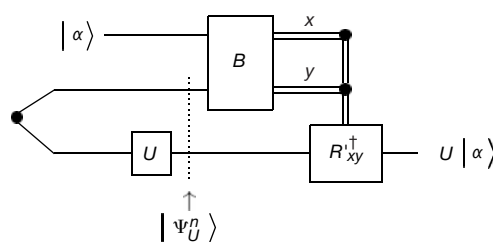
Operators from the Pauli group (such as X, Y and Z) can readily be performed on logical qubits which are encoded with a stabilizer code[18]. Let C_1 represent the Pauli group. C_2, the Clifford group, will be the set of gates which map Pauli operators into Pauli operators under conjugation. Through an appropriate sequence of gates and measurements, any C_2 operation can also be performed on any stabilizer code[18].

More difficult to perform are gates in the class defined as $C_3 \equiv \{U|UC_1U^\dagger \subseteq C_2\}$. C_3 contains gates such as the Toffoli gate (controlled-controlled-NOT), the $\pi/8$ gate (rotation about the Z-axis by an angle $\pi/4$), and the phase gate (diag$(1, 1, 1, i)$). Fault-tolerant constructions of these gates are known[7,8,19], but they are *ad hoc* and do not generalize easily.

However, our teleportation construction provides a straightforward way to produce any gate in C_3, as shown in Fig. 4. For $U \in C_3$, first construct the state $|\Psi_U^n\rangle = (I \otimes U)|\Psi^n\rangle$. Next, take the input state $|\Psi\rangle$ and do Bell basis measurements on this and the n upper qubits of $|\Psi_U^n\rangle$, leaving n qubits in the state $|\psi_{out}\rangle = UR_{xy}|\psi\rangle = R'_{xy}U|\psi\rangle$, where R_{xy} is an operator in C_1 which depends on the (random) Bell-basis measurement outcomes xy, and $R'_{xy} = UR_{xy}U^\dagger$ is an operator in C_2. As R'_{xy} is in the Clifford group, it can be performed—or more precisely, inverted—fault-tolerantly.

Creating $|\Psi_U^n\rangle$ may appear, at first sight, to be as difficult as performing U. However, constructing specific known states is easier than doing operations on unknown states: if the construction of an ancilla fails, little is lost by discarding the ruined state and starting again. This option is not available when we try to perform logical gate operations on actual data.

Our construction of quantum gates using teleportation offers possibilities for relaxing experimental constraints on realizing quantum computers. For example, using single photons as qubits and current optical technology, one can perform nearly perfect Bell-basis measurements[20], quantum teleportation[21], almost create GHZ states[22], and certainly perform single-qubit operations[23]. Thus, given GHZ states, quantum computers might be constructed almost completely from linear optical components. Our results

have similar implications for other physical systems, particularly if entangled states can readily be prepared and stored.

The Toffoli gate or another gate in C_3 is required for a universal fault-tolerant quantum computer, and our construction using teleportation offers a conceptual simplification over previous constructions. As with earlier realizations, our construction relies on the ability to create certain ancilla states $|\Psi_U^n\rangle$ which are independent of the data being acted upon. This means they may be prepared off-line, so $|\Psi_U^n\rangle$ are valuable generic quantum resources, perhaps a kind of 'quantum software', which might be considered a commercial commodity that could be manufactured. Even if states $|\Psi_U^n\rangle$ are not available, the construction can in some cases greatly reduce the number of operations needed to assemble the precise gates called for in an algorithm; this is of benefit in efficiently performing quantum computation with realistically imperfect gates. □

1. Shor, P. in *Proc. 35th Annu. Symp. on Foundations of Computer Science* (ed. Goldwasser, S.) 124–134 (IEEE Computer Society Press, Los Alomitos, 1994).
2. Grover, L. K. Quantum computers can search arbitrarily large databases by a single query. *Phys. Rev. Lett.* **79,** 4709–4012 (1997).
3. Preskill, J. Reliable quantum computers. *Proc. R. Soc. Lond. A* **454,** 385–410 (1998).
4. Steane, A. M. Efficient fault tolerant quantum computing. *Nature* **399,** 124–126 (1999).
5. Gottesman, D. Theory of fault-tolerant quantum computation. *Phys. Rev. A* **57,** 127–137 (1998).
6. Preskill, J. Quantum computing: pro and con. *Proc. R. Soc. Lond. A* **454,** 469–486 (1998).
7. Shor, P. W. in *Proc. 37th Annu. Symp. on Foundations of Computer Science* (IEEE Computer Society Press, Los Alamitos, 1996).
8. Knill, E., Laflamme, R. & Zurek, W. Resilient quantum computation. *Science* **279,** 342–345 (1998).
9. Bennett, C. H. *et al.* Teleporting an unknown quantum state via dual classical and EPR channels. *Phys. Rev. Lett.* **70,** 1895–1899 (1993).
10. Greenberger, D., Horne, M., Shimony, A. & Zeilinger, A. Bell's theorem without inequalities. *Am. J. Phys.* **58,** 1131–1143 (1990).
11. Brassard, G. in *PhysComp 96* (eds Toffoli, T., Biafore, M. & Leao, J.) 48–50 (New England Complex Systems Inst., Cambridge, Massachusetts, 1996).
12. Gottesman, D. in *Group22: Proc. XXII Int. Colloquium on Group Theoretical Methods in Physics* (eds Corney, S. P., Delbourgo, R. & Jarvis, P. D.) 32–43 (International Press, Cambridge, Massachusetts, 1999).
13. Nielsen, M. A. & Chuang, I. L. Programmable quantum gate arrays. *Phys. Rev. Lett.* **79,** 321–324 (1997).
14. Barenco, A. *et al.* Elementary gates for quantum computation. *Phys. Rev. A* **52,** 3457–3467 (1995).
15. Calderbank, A. R., Rains, E. M., Shor, P. W. & Sloane, N. J. A. Quantum error correction and orthogonal geometry. *Phys. Rev. Lett.* **78,** 405–408 (1997).
16. Steane, A. M. Multiple particle interference and quantum error correction. *Proc. R. Soc. Lond. A* **452,** 2551–2576 (1996).

17. Steane, A. M. Error correcting codes in quantum theory. *Phys. Rev. Lett.* **77,** 793–797 (1996).
18. Gottesman, D. *Stabilizer Codes and Quantum Error Correction.* Thesis, California Inst. of Technol. (1997).
19. Boykin, P. O., More, T., Pulver, M., Roychowdhury, V. & Vatan, F. On universal and fault-tolerant quantum computing. Preprint quant-ph/9906054 (cited June 1999) at ⟨http://xxx.lanl.gov⟩ (1999).
20. Kwiat, P. G. & Weinfurter, H. Embedded Bell-state analysis. *Phys. Rev. A* **58,** R2623–R2626 (1998).
21. Bouwmeester, D. *et al.* Experimental quantum teleportation. *Nature* **390,** 575–579 (1997).
22. Bouwmeester, D. *et al.* Observation of three-photon Greenberger-Horne-Zeilinger entanglement. *Phys. Rev. Lett.* **82,** 1345–1349 (1999).
23. Chuang, I. L. & Yamamoto, Y. Simple quantum computer. *Phys. Rev. A* **52,** 3489–3496 (1995).

Figure 1 TEM image showing ordered chains of prismatic BaCrO$_4$ nanoparticles. The nanoparticles were prepared in AOT microemulsions at [Ba^{2+}] : [CrO$_4^{2-}$] molar ratio $\approx$1 and w = 10. Scale bar = 50 nm.

....

Coupled synthesis and self-assembly of nanoparticles to give structures with controlled organization
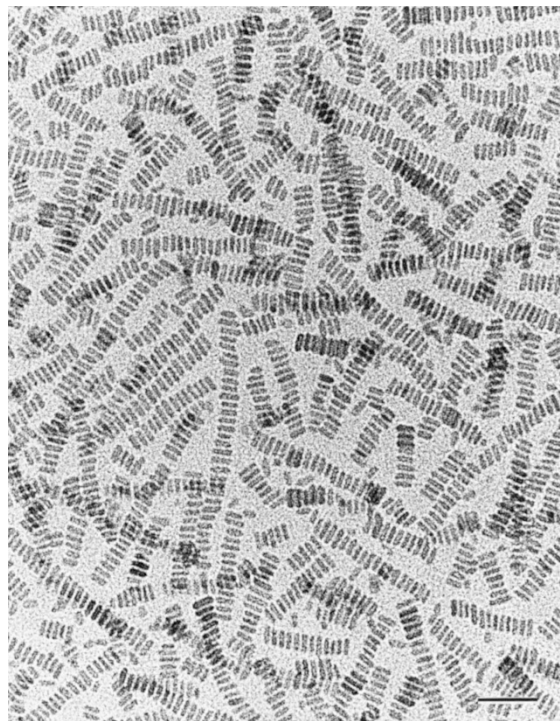
Mei Li*, **Heimo Schnablegger**† & **Stephen Mann***

* *School of Chemistry, University of Bristol, Bristol BS8 1TS, UK*
† *Max-Planck-Institut of Colloids and Interfaces, Am Muehlenberg, D-14476 Golm, Germany*

....

Colloidal inorganic nanoparticles have size-dependent optical, optoelectronic and material properties that are expected to lead to superstructures with a range of practical applications[1,2]. Discrete nanoparticles with controlled chemical composition and size distribution are readily synthesized using reverse micelles and microemulsions as confined reaction media[3–5], but their assembly into well-defined superstructures amenable to practical use remains a difficult and demanding task. This usually requires the initial synthesis of spherical nanoparticles, followed by further processing such as solvent evaporation[6–8], molecular cross-linking[9–14] or template-patterning[15–18]. Here we report that the interfacial activity of reverse micelles and microemulsions can be exploited to couple nanoparticle synthesis and self-assembly over a range of length scales to produce materials with complex organization arising from the interdigitation of surfactant molecules attached to specific nanoparticle crystal faces. We demonstrate this principle by producing three different barium chromate nanostructures—linear chains, rectangular superlattices and long filaments—as a function of reactant molar ratio, which in turn is controlled by fusing reverse micelles and microemulsion droplets containing fixed concentrations of barium and chromate ions, respectively. If suitable soluble precursors and amphiphiles with headgroups complementary to the crystal surface of the nanoparticle target are available, it should be possible to extend our approach to the facile production of one-dimensional 'wires' and higher-order colloidal architectures made of metals and semiconductors.

Barium bis(2-ethylhexyl)sulphosuccinate (Ba(AOT)$_2$) reverse micelles were added to sodium chromate (Na$_2$CrO$_4$)-containing NaAOT microemulsion droplets, to give final molar ratios of [Ba^{2+}] : [CrO$_4^{2-}$] $\approx$ 1 and water content w = [H$_2$O] : [NaAOT] = 10. This produced a yellow precipitate ~3 h after addition of the reactants at 25 °C. Transmission electron microscopy (TEM) images of samples taken directly from the liquid phase of the micro-

emulsion showed chain-like arrays that contained up to 60 nanoparticles (Fig. 1). The colloidal chain structures were 50–500 nm in length and consisted of rectangular-shaped particles that were uniform in length (mean = 16.0 ± 1.5 nm) and width (mean = 6.0 ± 0.4 nm), and preferentially aligned so that the long axis of each particle was perpendicular to the chain direction. Energy dispersive X-ray analysis and powder electron diffraction patterns indicated that the nanoparticles were crystalline BaCrO$_4$ with an orthorhombic unit cell (a = 0.911, b = 0.554, c = 0.734 nm). Each crystal along the length of the chain was separated by a regular spacing of 2 nm, consistent with the presence of an interdigitated layer of surfactant molecules.

Corresponding TEM studies on the sedimented material showed thin flake-like aggregates of a two-dimensional superlattice constructed from a pseudo-rectangular (90° $\leqslant$ θ $\leqslant$ 100°) array of uniformly sized BaCrO$_4$ nanoparticles that were separated by an interparticle spacing of 2 nm (Fig. 2). Thermal analysis indicated that the superlattices contained ~30% by weight of surfactant. Images of tilted lattices indicated that the particles were prismatic and identical to those present in the chain motif, and aligned with their long axis perpendicular to the plane of the superlattice. Viewed in-plane, the nanoparticles were rectangular in shape with mean dimensions of 6.8 ± 0.6 nm and 5.9 ± 0.5 nm, indicating two different types of side face. Electron diffraction failed to identify unequivocally the crystallographic nature of the side faces because of multiple arcing of the reflections arising from long-range disorder in the air-dried structures. However, patterns recorded from particles in the superlattice structure were indexed according to a superimposition of directions close to the [100] zone axis, which indicated that the prismatic crystals were single-domain particles elongated along the crystallographic a axis. This was consistent with a morphology based on a set of {100} end faces with {010} and {001} side faces.

Systematic changes in the water content (5 $\leqslant$ w $\leqslant$ 20), and hence